Numerical Prediction and Measurement of ESD Radiated Fields by Free-Space Field Sensors

Spartaco Caniggia, *Member, IEEE*, and Francescaromana Maradei, *Senior Member, IEEE*

***Abstract*—This paper describes the evaluation of electric and magnetic fields due to electrostatic discharges (ESDs) using an efficient numerical prediction model and measurements obtained with simple field sensors. The numerical prediction model is implemented using software based on the finite integration technique (FIT). The ESD generator is efficiently modeled, and the contact-mode discharge current is well reproduced taking into account the loading effect of the generator. Simple free-space field sensors are effectively used to measure the fields from an ESD event. Suitable numerical and theoretical characterizations of these sensors are proposed to derive a sensor transfer function that permits the fields to be reconstructed from the measured voltage. The numerical characterization is performed by Microwave Studio (MWS), while the theoretical characterization is based on lumped element circuit models of the sensors. The validation of both the proposed procedures indicates good accuracy up to 2 GHz as required by the International Electrotechnical Commission standard for ESD measurements.**

***Index Terms*—Electromagnetic interference (EMI), electrostatic discharge (ESD), finite integration technique (FIT), free-space field sensors, numerical modeling, radiated field.**

I. Introduction

ELECTROSTATIC discharge (ESD) is a natural phenomenon that can cause failures and/or damage to electronic equipment. The current discharge produced by a human metal event has significant spectral components up to 2 GHz due to the fast rise time of the current waveform, often less than 1 ns. This paper describes an efficient numerical prediction model, and establishes a free-space field sensor measurement procedure for evaluating the electromagnetic fields radiated by an ESD event.

Several papers describing the calculation and measurement of ESD radiated fields have been published. A relatively simple dipole model of an ESD spark was developed in [1]. However, this model does not take into account the other currents produced by an ESD generator, such as the internal current of the relay in a contact-mode discharge, the displacement current between the body of the ESD generator and nearby metal parts, and the return strap current. For these reasons, the agreement between theory and measurements is poor.

Cerri *et al*. [2], [3] have shown that commercial field probes can be effectively used to measure the radiated field generated by an ESD event. The field can be derived from the measured data by applying a procedure based on a knowledge of the sensor transfer function of the field probes. A TEM-horn cell was used to obtain the transfer function of magnetic field sensor. Cerri *et al*. [4] have also shown that a numerical approach can be used to compute radiated fields. However, the radiating structures considered were limited to a monopole and a loop.

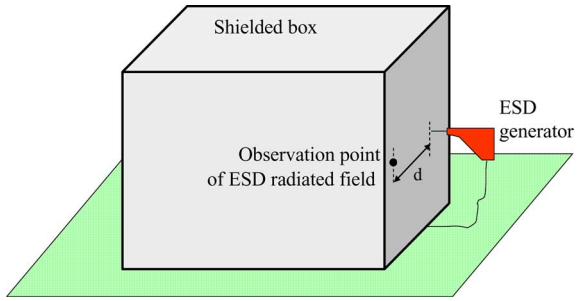

Fig. 1. Test setup to evaluate the ESD radiated field.

In [5]–[7], the ESD current and the transient radiated fields are simulated using the finite-difference time-domain (FDTD) method. This approach takes into account the contribution of all the currents involved in radiating fields, since the body of the ESD generator with its lumped elements and the position of the ground strap can be simulated with great accuracy.

Recently, Pommerenke *et al*. [8], [9] have shown that for ESD generators built in accordance with International Electrotechnical Commission (IEC) 61000-4-2 specifications [10], the voltage induced in a small loop correlates with the failure level observed in an ESD test on systems composed of fast CMOS devices, while the rise time and derivative of the discharge current do not correlate well. These results demonstrate the importance of modeling and measuring the radiated fields associated with an ESD event. The maintenance group MT12 of IEC, in charge of preparing the second edition of this specification, has acknowledged this point, and has decided to prepare an informative Annex D regarding the radiated field effects produced by ESD events [11].

In this paper, an efficient numerical model of the ESD test setup shown in Fig. 1 is developed. It is implemented using the software tool Microwave Studio (MWS) based on the finite integration technique (FIT) [12]. The model accounts for the ESD generator, and can accurately simulate the discharge current taking into account the geometry and the loading effect of the generator. A simple procedure is, then, proposed to measure electric and magnetic fields from ESD generators using free-space sensors. The characterization of the field sensors is performed by numerical simulations and by a

Manuscript received March 22, 2006; revised July 17, 2006 and November 28, 2006. This work was supported in part by Italtel S.p.A.

S. Caniggia is an EMC Consultant, 20010 Bareggio, Italy (e-mail: spartaco.caniggia@ieee.org).

F. Maradei is with the Department of Electrical Engineering, "La Sapienza" University of Rome, 00184 Rome, Italy (e-mail: fr.maradei@ieee.org).

Color versions of one or more of the figures in this paper are available online at http://ieeexplore.ieee.org.

Digital Object Identifier 10.1109/TEMC.2007.902196

simplified theoretical approach. It will be shown that the ESD-radiated field measurements are in good agreement with the numerical simulations, even when the free-space sensors are characterized using the simplified approach.

The paper is organized as follows. Section II provides a detailed description of the ESD generator numerical model. Section III explains the experimental setup used in the measurements. Sections IV and V describe the calibration of the free-space field sensors using numerical simulations and a simplified theoretical approach. Finally, the validation of the proposed calibration procedures and comparisons between numerical results and measurements are presented in Section VI.

II. Numerical Model of ESD Test Setup

ESD generators are commonly used to test for immunity to ESD, and their purpose is to reproduce typical human metal discharges. To this aim, most generators are built in compliance with the specification contained in IEC 61000-4-2 [10]. In general, the discharge current depends on the impedance of the target where the discharge event occurs.

The accurate and efficient modeling of the generator is a critical aspect of ESD immunity modeling and the numerical simulation of ESD fields. It is essential to account for the loading effect of the generator. The test setup for current calibration described in the new IEC 61000-4-2 proposal [12] was used to evaluate an MWS model of the ESD generator. This test setup models the ESD event on a conductive wall. The experimental setup was arranged in the shielded room of Italtel S.p.A. as shown in Fig. 2(a). The measurement of the ESD current is performed by using the current sensing transducer highlighted in the figure. The construction of the resistive load behaving as a current transducer is described in [11]. The wall is on one side of a shielded enclosure in which a target is mounted to measure currents on a digital oscilloscope within the enclosure. This configuration avoids coupling between the ESD event and the instrumentation. All the measurements are carried out at a charging voltage of 5 kV, and with an oscilloscope that has a 2-GHz bandwidth. The flat ESD strap is connected to the metallic wall where the discharge occurs.

The MWS model shown in Fig. 2(b) contains dielectric parts, metallic parts, and lumped circuit elements that reproduce the physical form of a typical ESD generator and the reference discharge current [11] proposed by the IEC 77B MT12 group.

The ESD generator geometry adopted for the numerical simulation is similar to the one reported in [6]. It is suitable for reproducing the reference ESD current defined in [11], and it is consistent with the DITO generator construction [13]. The material properties used to model the different parts of the ESD gun are shown in Fig. 3. The lumped circuit elements adopted in the MWS model are shown in Fig. 4.

Some remarks are required to clarify the excitation used in the numerical model to simulate the discharge event. In practice, the generator is first charged to 5 kV, then a relay that operates in a few picoseconds, puts the two parts of the generator in contact, establishing a short circuit and allowing the circulation of the discharge current. From a numerical point of view, this

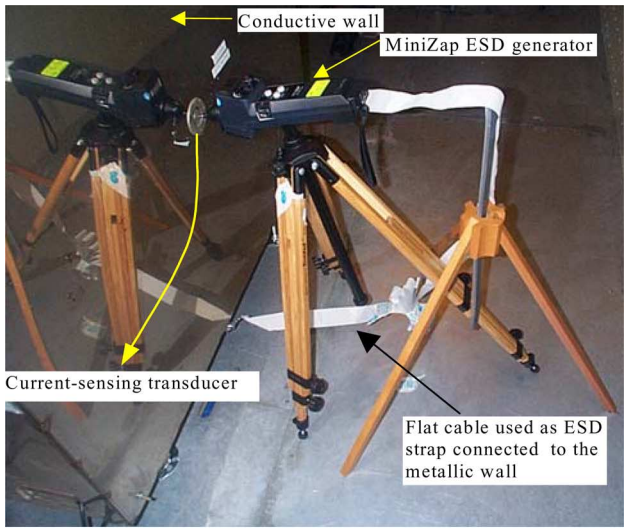

(a)

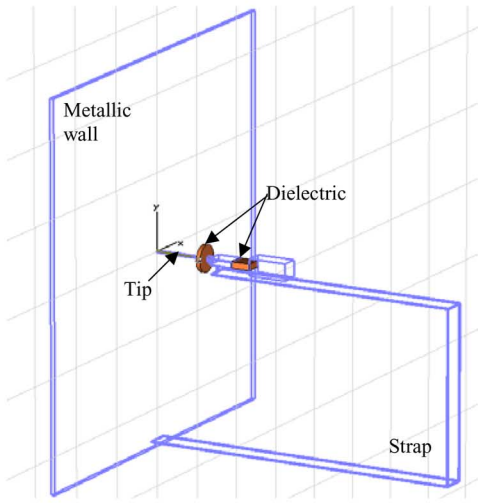

(b)

Fig. 2. Test setup used for (a) ESD current calibration and (b) corresponding ESD generator configuration modeled by MWS.

generator can not be simulated in a straightforward manner, since the software only allows a unit-step current source to switch from zero to one. Here, the model is excited at port 2 (see Fig. 4) by an ideal current source with a 25-Ω source impedance assuming a step rise-time of 1 ns to reproduce the actual slow charging, switching, and rapid discharge process of an ESD generator. In order to reproduce the actual values of the discharge current, a normalization factor $f_n = -500$ must be applied. The minus sign is due to the fact that numerically the discharge event simulates the passage from 0 to 10 V at the terminals of port 2 instead of the passage from 5 to 0 kV, (i.e., $f_n = -5000/10$). Note that the MWS simulation does not model the RF pulse formation occurring in the ESD generator. In a real ESD generator, there are lots of parts that increase the rise time from picoseconds at the relay to nanoseconds at the tip. These phenomena are not included in the proposed MWS model. The shape of the excitation waveform performs the switching.

The tip and strap current obtained by the MWS model are shown in Figs. 5 and 6. The measurements were performed

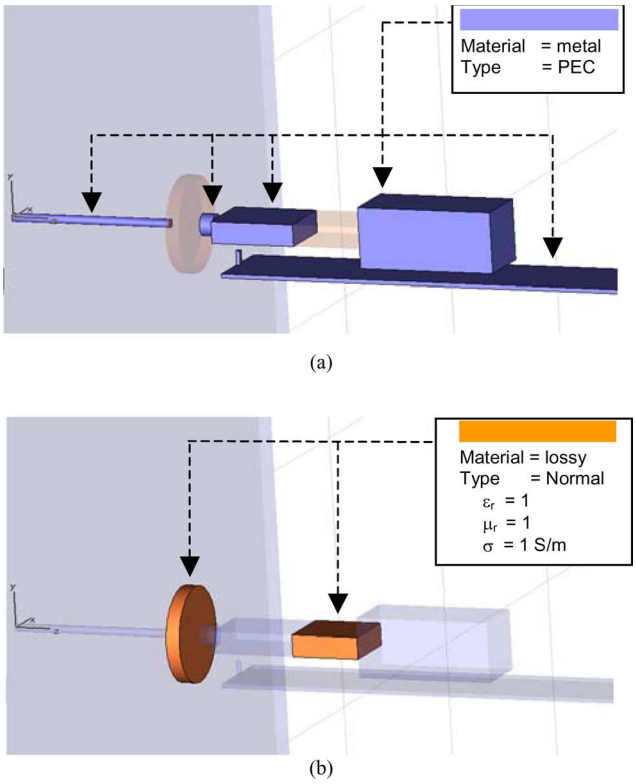

Fig. 3. Material details of the ESD generator model in MWS. (a) Perfect electric conductive region. (b) Lossy dielectric regions.

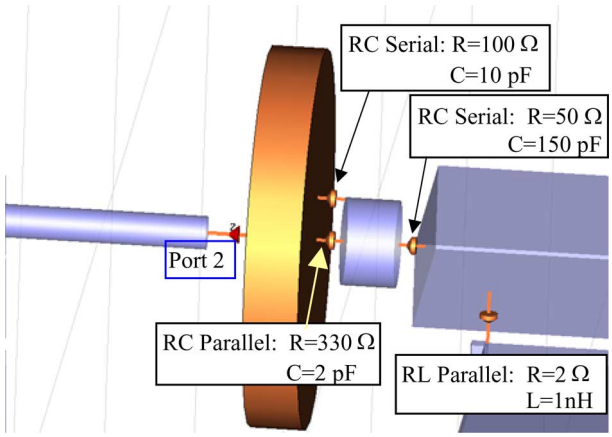

Fig. 4. Lumped element network and port excitation used to reproduce the physical form of a typical ESD generator and the reference discharge current proposed.

by using a MiniZap commercial ESD generator [14] to assess the agreement with the numerical model based on the ESD DITO generator. The comparison between the simulation results and the measurements exhibits good agreement. Moreover, the following observations can be made.

- The first fast rise time (less than 1 ns) is reproduced, and closely matches the reference IEC current.
- The measured and simulated waveforms after the first peak are similar with slight oscillations in the reference IEC current.

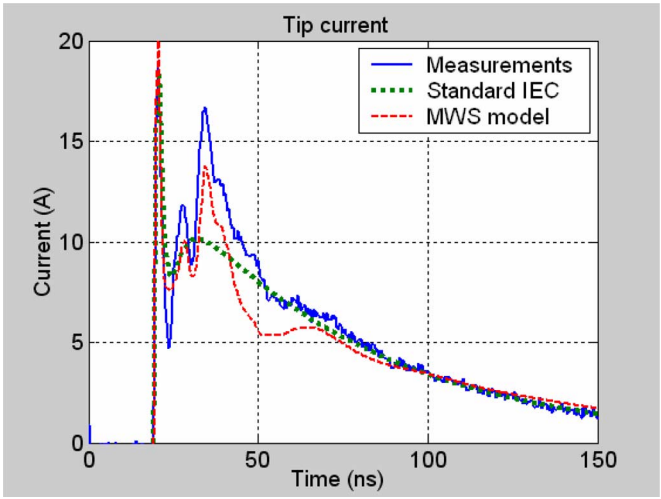

Fig. 5. Tip current occurring in the test setup for current calibration: measurements (solid line); standard IEC ESD current (dotted line); MWS model (dashed line).

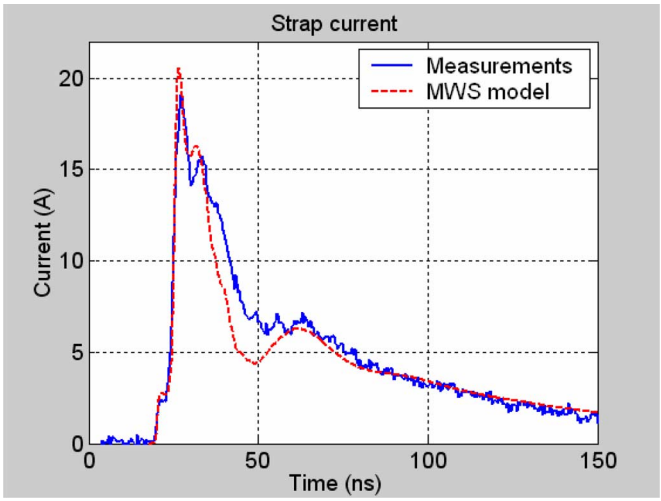

Fig. 6. Strap current occurring in the test setup for current calibration: measurements (solid line); MWS model (dashed line).

- The current on the strap has a slower rise time than the current on the tip. This is due to the capacitance between the ESD generator and the environment that permits an alternative path for the first peak of the ESD current.

To verify the numerical model in terms of the reproducibility of the test results, the calculated tip current is compared in Fig. 7 with the results of measurements performed using the MiniZap generator twice and using the DITO generator. Satisfactory agreement is observed. In particular, the accuracy of the first peak is very good while some discrepancies occur on the falling edge. It is worth noting that the reproducibility of the second peak with better accuracy and the reduction of the falling edge ringing is an open problem to which the IEC committee is addressing significant attention [11]. The ringing of the discharge current depends on the type of ESD generator. A main goal of the IEC committee is to set up specifications for ESD generator manufactures in order to improve test result

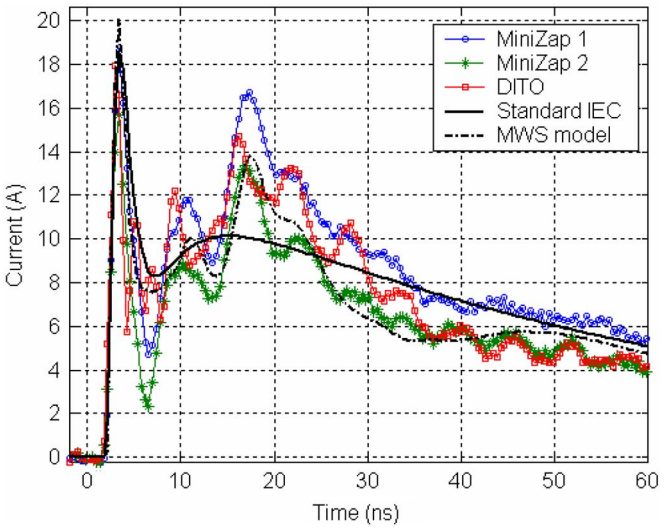

Fig. 7. Transient tip current occurring in the test setup of Fig. 1 obtained by measurements using different ESD generators and by the proposed numerical model.

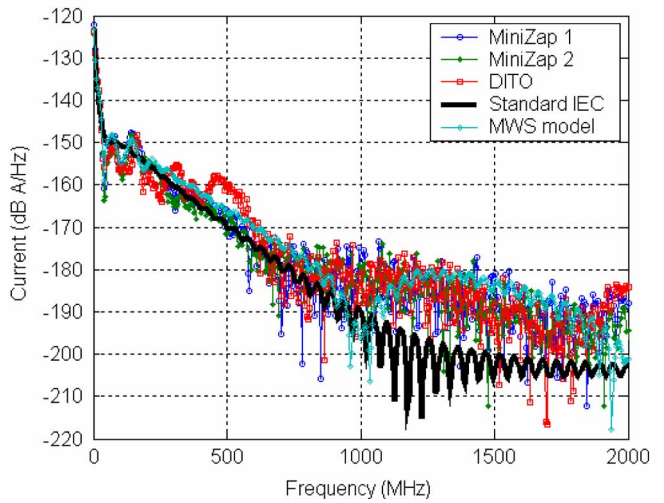

Fig. 8. Spectral content of the tip current occurring in the test setup of Fig. 1 obtained by measurements using different ESD generators and by the proposed numerical model.

reproducibility. The present lack of standardization capable of assuring satisfactory reproducibility of the ESD current falling edge leads to even more evident discrepancies in the current spectral content. Measured and calculated tip current spectral content are shown in Fig. 8, where some differences are evident. Nevertheless, these ESD generators satisfy the requirements defined in [10].

III. Setup to Measure the ESD-Radiated Fields Using Free-Space Sensors

The test setup used to measure the electric and magnetic fields radiated by an ESD event is shown in Fig. 9. The setup was arranged in a shielded room to avoid interference from the environment, and includes the following:

- ESD generator at 5 kV;
- digital oscilloscope of bandwidth at least 2 GHz;
- set of free-space H-field (small loop with shield) and E-field (small monopole) probes; and
- 50-Ω coaxial cable.

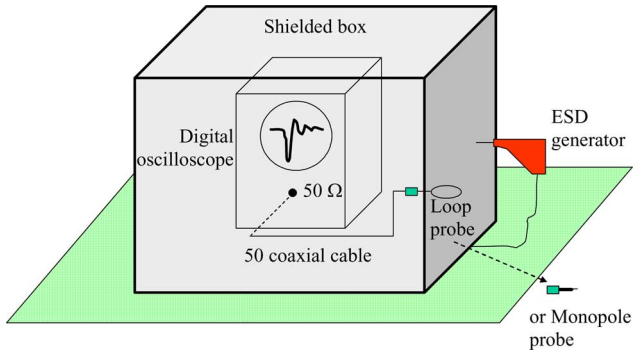

Fig. 9. Example of test setup to measure the ESD radiated field.

The ESD event occurs on the external side of the shielded enclosure connected to the metallic floor of the shielded room. To avoid the coupling between the ESD event and the instrumentation, the digital oscilloscope is placed within the shielded enclosure. The field probes characterized by reduced dimensions for minimum coupling with adjacent bodies are connected to the oscilloscope by a 50-Ω coaxial cable, and positioned at the edge of the shielded box as shown in Fig. 9. This setup prevents possible pick up of radiated fields by the coaxial cable. In other possible test configurations where the cable could pick up disturbances, a preliminary measurement of the voltage at the input to the oscilloscope in absence of the field probe is required to evaluate the noise. If this noise is significant, the measurement should be repeated considering the following EMI practical fixes: change the cable routing; add ferrite or absorber to the cable, or use coaxial cable with better shielding performance. The measurement of the radiated field at different distances is carried out by shifting the position of the ESD discharge point.

The described setup measures the voltage $v\ (t)$ across the 50-Ω input of the oscilloscope due to the radiated fields produced by the ESD event. The calculation of the corresponding electric and magnetic fields would be straightforward with sensors characterized by a flat amplitude response over a wide frequency range with minimum phase distortion. However, sensors with such characteristics are not very common (i.e., not always available), and quite expensive. Here, our interest is focused on the measurement of ESD-radiated fields using simple sensors, such as electrically small loops with shields for E-rejection (H-field probes), and small monopoles (E-field probes).

In this case, starting from the oscilloscope voltage drop $v\ (t)$, the corresponding electric and magnetic fields can be derived by the following steps.

1) Calculation of the Fourier transform of the sensor output voltage

$$V(\omega) = F[v(t)]. \tag{1}$$

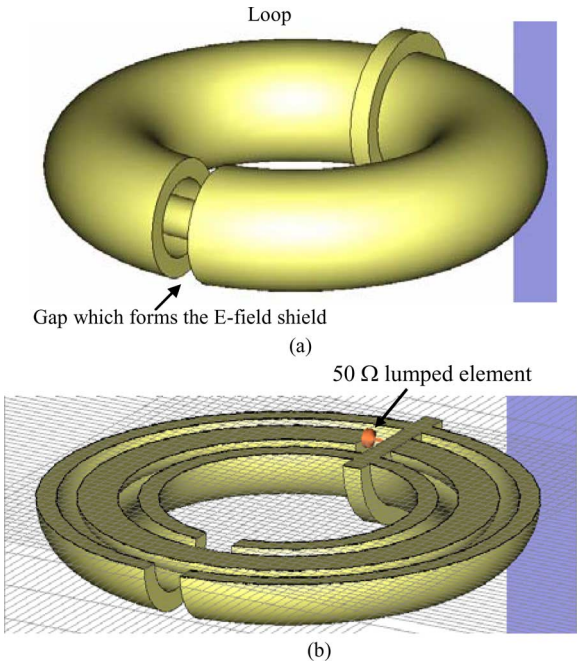

Fig. 10. (a) MWS model of the H-field sensor. (b) Detail of the mesh used in the simulation.

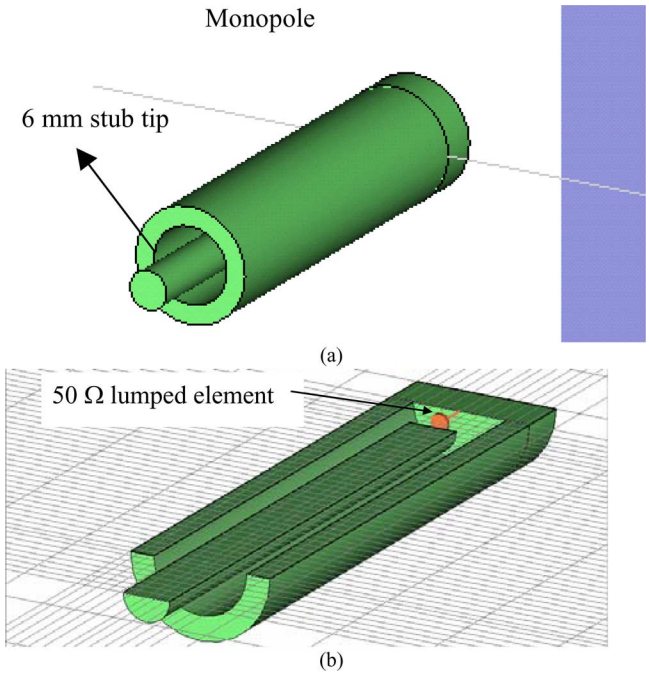

Fig. 11. (a) MWS model of the E-field sensor. (b) Detail of the mesh used in the simulation.

2) Calibration of the field sensor to carry out the probe transfer function $T(\omega)$ defined as

$$T(\omega) = \frac{V(\omega)}{F(\omega)} \tag{2}$$

where $F(\omega)$ is the incident field, which can be either H or E, and $V(\omega)$ is the voltage drop across the 50-Ω input during the calibration procedure.

3) Calculation of the corresponding transient field $f(t)$ by the inverse Fourier transform as

$$f(t) = F^{-1}\left[\frac{V(\omega)}{T(\omega)}\right]. \tag{3}$$

The calibration of the field sensor [i.e., the derivation of the probe transfer function $T(\omega)$], can be performed either numerically or analytically by using a plane-wave source with the fields oriented as generated by the ESD generator. The two calibration procedures are described in Sections IV and V.

IV. Calibration of Free-Space Sensors by Numerical Simulations

The calibration of the H- and E-field sensors was performed by modeling the sensors with the commercial software tool MWS [12]. The H-field probe was a 3-cm loop consisting of an internal ring terminated at a 50-Ω resistance and an open external ring electrically connected to the internal one, acting as an electrostatic shield. The MWS model of the H-field sensor is shown in Fig. 10. The calibration of the H-field probe is performed by exciting the probe with a plane-wave field polarized with the H-field perpendicular to the loop, and calculating the voltage on the 50-Ω resistance.

The monopole E-field probe consisted of a 6-mm stub tip with a partial shield. The sensor configuration and the mesh used for the simulation are shown in Fig. 11. The calibration of the E-field probe was performed by exciting the probe with a plane wave polarized with the E-field parallel to the monopole.

It should be noted that due to the setup configuration (i.e., Fig. 9), and in particular to the position of the coaxial cable, which is not directly illuminated by the ESD radiated field, the numerical characterization of both the field sensors was performed by simply modeling the coaxial cable connection to the oscilloscope using a 50-Ω lumped load.

The transfer function calculation of both H- and E-field probes was performed with suitable local subgridding (see Figs. 10 and 11) in order to assure good accuracy with reasonable computational resources.

V. Calibration of Commercial Sensors by a Simplified Theoretical Approach

A simplified analytical approach for calibrating the sensors using equivalent lumped circuits is proposed. This approach is efficient and accurate as long as the dimensions of the probe D_{probe} are much less than the minimum wavelength of interest $\lambda_{\min}$.

A. Simplified Analytical Calibration of H-Field Probe

The H-field probe schematically shown in Fig. 12 can be described by the frequency-domain circuit equation

$$j\omega\mu_0 H(\omega) S_{\text{loop}} = j\omega L_{\text{loop}} I_{\text{loop}}(\omega) + V_{\text{load}}(\omega) \tag{4}$$

where $H(\omega)$ is the normal magnetic field impinging on the probe, S_{loop} is the area of the loop, L_{loop} is the loop inductance,

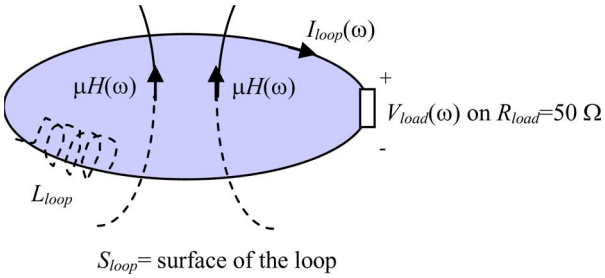

Fig. 12. Schematic representation of the H-field loop sensor.

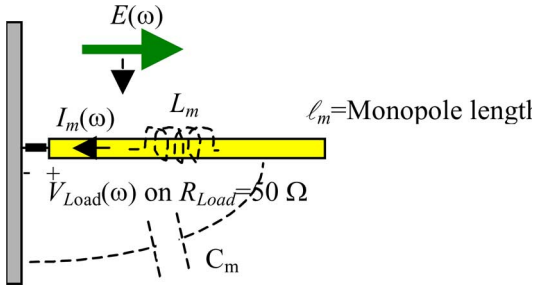

Fig. 13. Schematic representation of the E-field monopole probe.

$I_{\rm loop}(\omega)$ is the current circulating in the loop, and $V_{\rm load}(\omega)$ is the measured voltage. Due to the presence of the electric-field shield, only the effect of the magnetic field has been taken into account. Equation (4) can be rewritten as

$$j\omega\mu_0 H(\omega) S_{\rm loop} = j\omega L_{\rm loop} \frac{V_{\rm load}(\omega)}{R_{\rm load}} + V_{\rm load}(\omega) \qquad (5)$$

where $R_{\rm load}$ is the 50-Ω load impedance of the instrument.

The loop inductance $L_{\rm loop}$ in (5) is given by [15]

$$L_{\rm loop} = \mu_0 r_{\rm loop} \left(\ln \left(\frac{8 r_{\rm loop}}{r_{\rm wire}} \right) - 1.75 \right) \qquad (6)$$

where $r_{\rm loop}(= 1.4$ cm) is the inner radius of the H-field loop, and $r_{\rm wire}(= 0.15$ cm) is the radius of the loop wire. By simple manipulations on (5), the H-field probe transfer function is derived as

$$T_H(\omega) = \frac{V_{\rm load}(\omega)}{H(\omega)} = \frac{j\omega\mu_0 S_{\rm loop}}{1 + j\omega L_{\rm loop}/R_{\rm load}}. \qquad (7)$$

B. Simplified Analytical Calibration of E-Field Probe

Adopting the schematic representation shown in Fig. 13, where the E-field probe is modeled by a simple monopole, the frequency-domain circuit equation can be obtained as

$$E(\omega)\ell_m = j\omega L_m I_m(\omega) + \frac{1}{j\omega C_m} I_m(\omega) + V_{\rm load}(\omega) \qquad (8)$$

where $E(\omega)$ is the incident electric field tangent to the monopole, $\lambda_m(= 0.6$ cm) is the monopole length, and L_m and C_m are the monopole inductance and capacitance, respectively. $I_m(\omega)$ is the monopole induced current, and $V_{\rm load}(\omega)$ is the measured voltage. In (8), the monopole inductance and capacitance are given by [16]

$$L_m = \frac{\mu_0 \ell_m}{3\pi} \left(\ln \left(\frac{2\ell_m}{r_{\rm wire}} \right) - \frac{11}{6} \right) \qquad (9a)$$

$$C_m = \frac{2\varepsilon_0 \varepsilon_r \ell_m \pi}{\ln(2\ell_m / r_{\rm wire})} \qquad (9b)$$

where $r_{\rm wire}(= 0.15$ cm) is the radius of the monopole wire.

Introducing Ohm's law $I(\omega) = V_{\rm load}(\omega)/ R_{\rm load}$, to (8) yields

$$E(\omega)\ell_m = \left[j\omega \frac{L_m}{R_{\rm load}} + \frac{1}{j\omega C_m R_{\rm load}} + 1 \right] V_{\rm load}(\omega). \qquad (10)$$

By simple manipulations on (10), the E-field probe transfer function is derived as

$$T_E(\omega) = \frac{V_{\rm load}(\omega)}{E(\omega)} = \frac{\ell_m}{j\omega \frac{L_m}{R_{\rm load}} + \frac{1}{j\omega C_m R_{\rm load}} + 1}. \qquad (11)$$

In practice, the actual monopole differs from the ideal configuration depicted in Fig. 13, due to the presence of the electrostatic shield, which acts as a reference ground. To take into account the actual shape of the E-field probe, it has been verified through numerical simulations that a factor 3.4 should be introduced in (9b) to obtain the actual probe capacitance C_m.

VI. Validation

The H-field and E-field probe transfer functions (i.e., $T_H(\omega)$ and $T_E(\omega)$, respectively), calculated by the full-wave numerical model described in Section IV and by the simplified analytical approach of Section V are shown in Figs. 14 and 15. The results obtained by the two procedures are in overall good agreement below 2 GHz, with the exception of a resonance in the H-field probe transfer function. This resonance cannot be reproduced by the simplified analytical model, and it is in agreement with the results presented in [4]. It is worth noting that the MWS models are capable of characterizing the sensors even at frequencies higher that 1 GHz while the simplified theoretical approach is no longer valid at those frequencies.

The ESD-radiated field measurement setup described in Section III and shown in Fig. 9, has been modeled by MWS using the ESD generator model developed in Section II, and the H- and E-field sensor models presented in Section V. The measured and calculated voltages induced in the field probes by an ESD event at different distances (i.e., 15 and 45 cm) are shown in Figs. 16 and 17, and good agreement can be observed. The corresponding H- and E-field spectral densities are shown in Figs. 18 and 19. Note that in the central part of the considered frequency range, there are differences of several decibels due to the ESD intrinsic generator waveform oscillations after the first peak, as shown in Fig. 7, and discussed in Section II.

The probe transfer functions obtained by the proposed analytical and numerical approaches are used to derive the radiated fields according to the procedure highlighted in Section III by (1)–(3). The measured magnetic and electric fields at different distances are shown in Figs. 20 and 21 together with the MWS results achieved without the presence of the field probes. The comparison shows that there is a very good agreement between

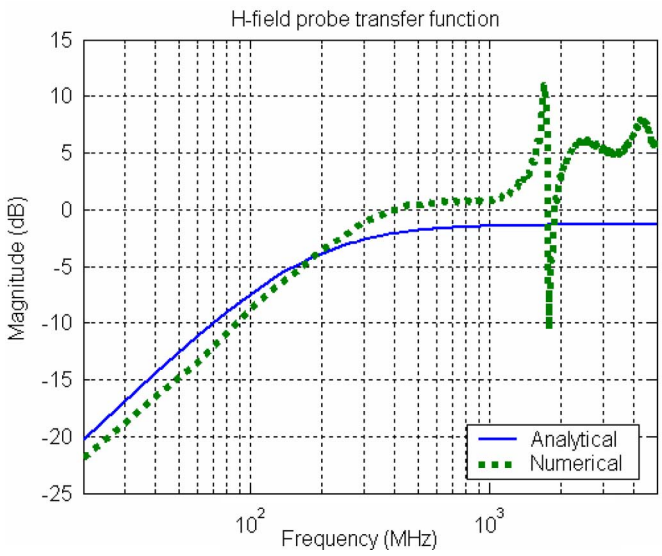

Fig. 14. H-field probe transfer function calculated by the analytical approach (continuous line) and by the software tool MWS (dotted line).

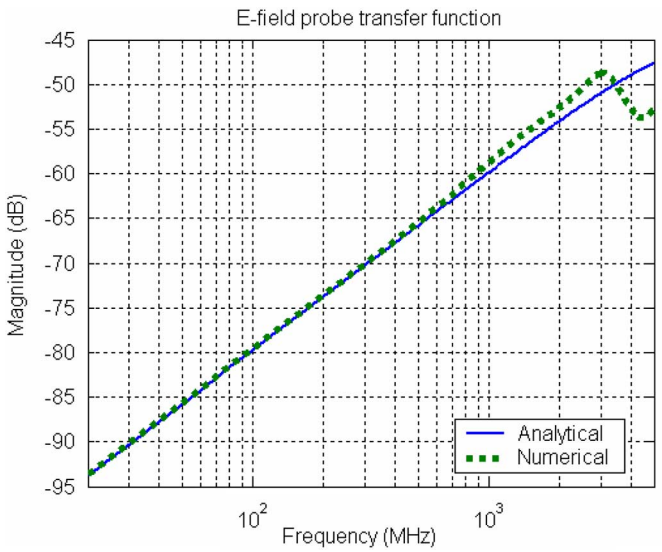

Fig. 15. E-field probe transfer function calculated by the software tool MWS (dotted line) and by the analytical approach (continuous line).

measurements and numerical results. In particular, it is worthy to note the satisfactory accuracy of the simplified analytical approach, despite the simple procedure used to find the probe transfer function. Moreover, since the analytical approach is only valid below 1 GHz, it is apparent that the accurate description of the free-space probe transfer function at frequencies higher that 1 GHz is not essential.

The peak values of the measured magnetic field are 3 A/m at 45 cm and 9 A/m at 15 cm. The peak values of the electric field are 2.2 kV/m at 45 cm, and 7.5 kV/m at 15 cm. In this setup, the ESD field is predominantly electric (i.e., high impedance source), at both distances evaluated. This can be easily verified by considering the ratio between the peak values of the electric and magnetic field, which is greater than the typical plane wave impedance (i.e., 377 Ω). Other simulations not reported in this

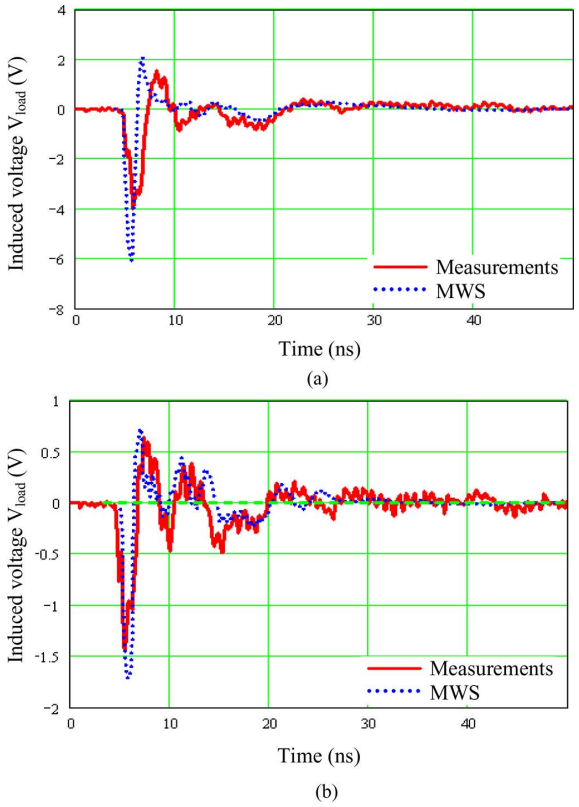

Fig. 16. Induced voltage in the H-field probe at a distance of (a) 15 cm and (b) 45 cm from the ESD event. Results were obtained by the software tool MWS (dotted line) and by measurements (continuous line).

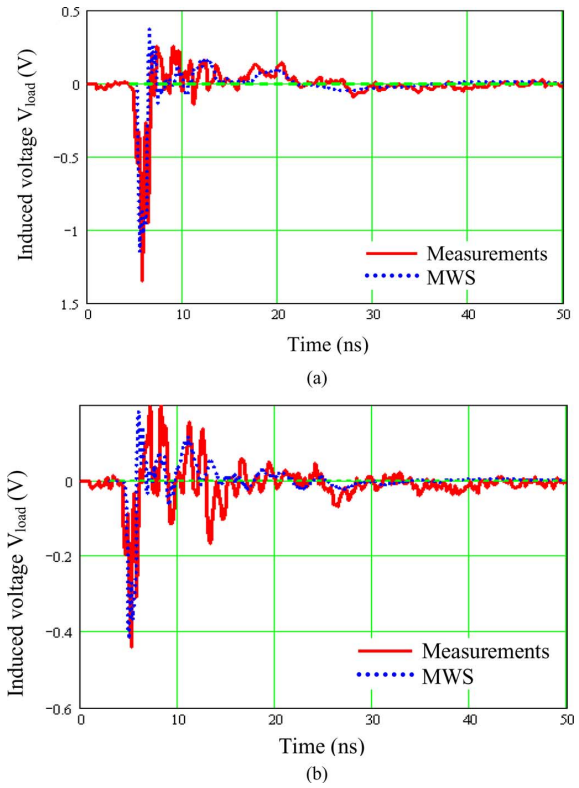

Fig. 17. Induced voltage in the E-field probe at a distance of (a) 15 cm and (b) 45 cm from the ESD event. Results were obtained by the software tool MWS (dotted line) and by measurements (continuous line).

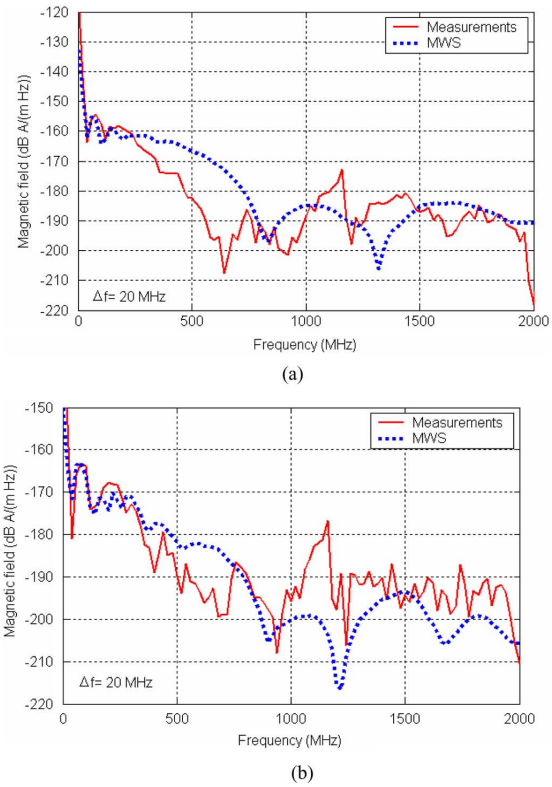

Fig. 18. H-field spectral density at a distance of (a) 15 cm and (b) 45 cm from the ESD event. Results were obtained by the software tool MWS (dotted line) and by measurements (continuous line).

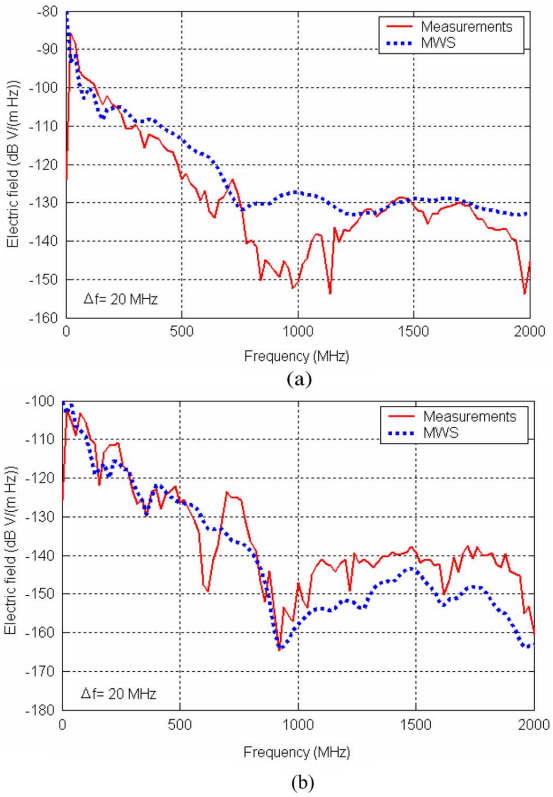

Fig. 19. E-field spectral density at a distance of (a) 15 cm and (b) 45 cm from the ESD event. Results were obtained by the software tool MWS (dotted line) and by measurements (continuous line).

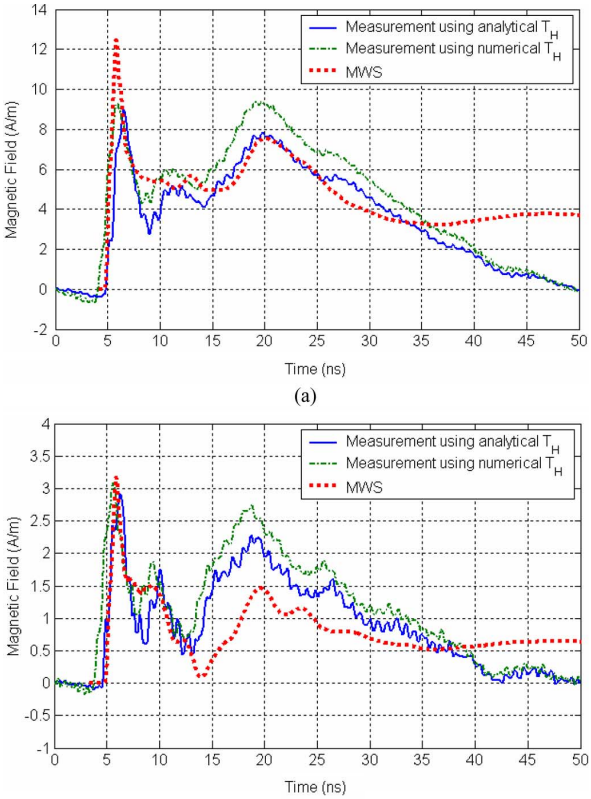

Fig. 20. Radiated magnetic field at a distance of (a) 15 cm and (b) 45 cm from the ESD event.

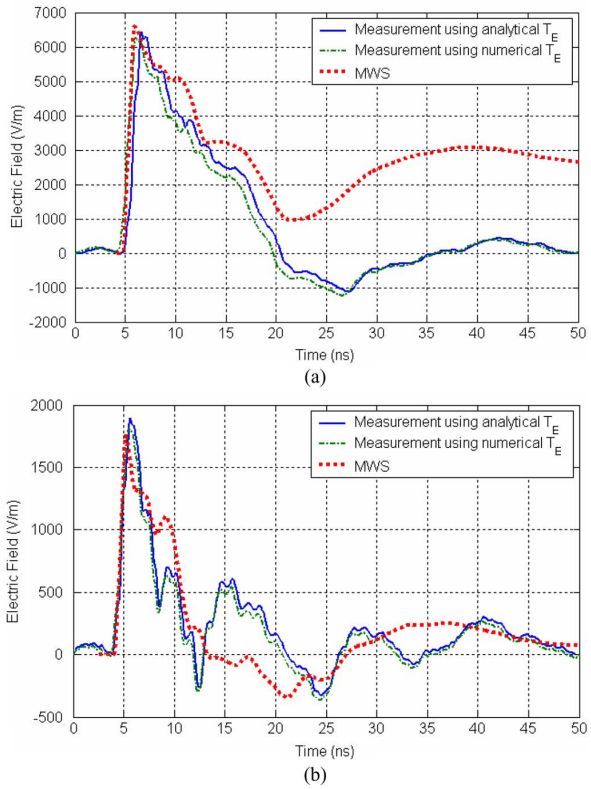

Fig. 21. Radiated electric field at a distance of (a) 15 cm and (b) 45 cm from the ESD event.

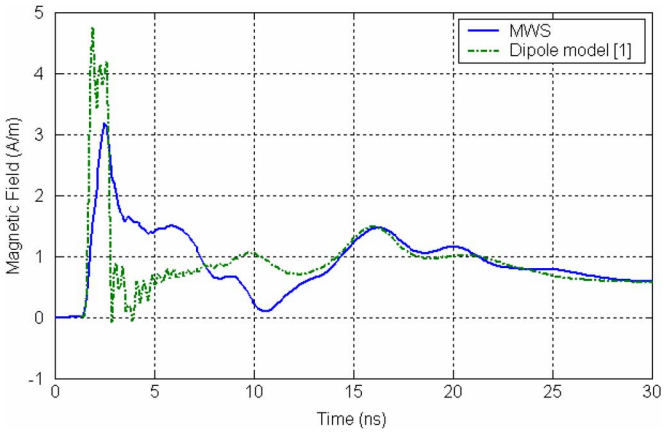

Fig. 22. Radiated magnetic field at a distance of 45 cm from the ESD event obtained by the developed MWS model (continuous line) and by the dipole model (dash-dotted line) [1].

paper, have verified that the far-field condition is respected when the probe is placed above an infinite metallic wall and not at the edge of a finite metallic wall.

A final point worth mentioning is the importance of accounting for the entire ESD current path distribution when determining the ESD fields. The radiated magnetic field, 45 cm from the ESD event, and obtained by MWS is compared in Fig. 22 with that calculated using the dipole model [1], in which the tip of the ESD is assumed to be the only radiating element and using the numerically calculated current. The results of Fig. 22 show that the model [1] leads to an overestimation of the first peak and a faster calculated rise time.

VII. Conclusion

Measurements of the fields associated with an ESD event were made using free-space H- and E-field probes, and compared with numerical results achieved using a suitable MWS prediction model. The transfer functions of the probes were calculated using a simple circuit approach and numerically using MWS, avoiding the complex procedure reported in [4] for H-probes and in [7]. The results obtained are in good agreement with the results reported in [7] and [8]. It has also been shown by comparing simulations and measured results that the fields from an ESD event can be numerically predicted with satisfactory accuracy.

Acknowledgment

The authors would like to thank L. Vitucci for helping with the experimental measurements, and D. Pommerenke for helpful discussions and valuable suggestions in the preparation of this paper.

References

[1] P. F. Wilson and M. T. Ma, "Fields radiated by electrostatic discharges," *IEEE Trans. Electromagn. Compat.*, vol. 33, no. 1, pp. 10–18, Feb. 1991.

[2] G. Cerri, R. De Leo, and V. Mariani Primiani, "Theoretical and experimental evaluation of electromagnatic fields radiated by ESD," in *Proc. IEEE Int. Symp. Electromagn. Compat.*, Montreal, QC, Canada, Aug. 13–17, 2001, pp. 1269–1272.

[3] G. Cerri, F. Coacci, L. Fenucci, and V. Mariani Primiani, "Measurement of magnetic fields radiated from ESD using field sensors," *IEEE Trans. Electromagn. Compat.*, vol. 43, no. 2, pp. 187–196, May 2001.

[4] G. Cerri, S. Chiarandini, S. Costantini, R. De Leo, V. Mariani Primiani, and P. Russo, "Theoretical and experimental characterization of transient electromagnetic fields radiated by electrostatic discharge (ESD) currents," *IEEE Trans. Electromagn. Compat.*, vol. 44, no. 1, pp. 139–147, Feb. 2002.

[5] D. Pommerenke, T. Van Doren, and W. Kai, "ESD currents and fields on the VCP and the HCP modeled using quasi-static approximations," in *Proc. IEEE Int. Symp. Electromagn. Compat.*, Minneapolis, MN, Aug. 18–23, 2002, pp. 81–86.

[6] S. Caniggia, F. Centola, D. Pommerenke, W. Kai, and T. Van Doren, "ESD exicitation model for susceptibility study," in *IEEE Int. Symp. Electromagn. Compat.*, Boston, MA, Aug. 18–22, 2003, pp. 58–63.

[7] K. Wang, D. Pommerenke, R. Chundru, T. Van Doren, J. Drewniak, and A. Shashindranath, "Numerical modeling of electrostatic discharge generators," *IEEE Trans. Electromagn. Compat.*, vol. 45, no. 2, pp. 258–271, May 2003.

[8] R. Chundru, D. Pommerenke, K. Wang, T. Van Doren, F. Centola, and J. Huang, "Characterization of human metal ESD reference discharge event and correlation of generator parameters to failure levels—Part I: Reference event," *IEEE Trans. Electromagn. Compat*, vol. 46, no. 4, pp. 498–504, Nov. 2004.

[9] K. Wang, D. Pommerenke, R. Chundru, T. Van Doren, F. Centola, and J. Huang, "Characterization of human metal ESD reference discharge Event and correlation of generator parameters to failure levels—Part II: Correlation of generator parameters to failure levels," *IEEE Trans. Electromagn. Compat.*, vol. 46, no. 4, pp. 505–511, Nov. 2004.

[10] IEC 61000-4-2, "EMC—Part 4-2-Ed: Testing and measurement techniques—ESD immunity test," 1995; Amendment 1: 1998; Amendment 2: 2001.

[11] 77B/491e/CD, "IEC 61000-4-2: EMC—Part 4-2: Testing and measurement techniques—ESD immunity test," Dec. 9, 2005.

[12] Microwave Studio, Computer Simulation Technology, [Online]. Available: www.cst.de

[13] Dito ESD generator, Amplifier Research Worldwide, [Online]. Available: http://www.arww-rfmicro.com/html/18200.asp?id=258

[14] Key Tek MiniZap ESD generator—Model MZ 15 EC, Termo Electron Corporation, [Online]. Available: http://www.thermo.com/com/cda/product/

[15] S. Ramo, J. R. Whinnery, and T. Van Duzer, *Fields and Waves in Communication Electronics*. Hoboken, NJ: Wiley, 1965.

[16] S. A. Schelkunoff and H. T. Friis, *Antennas: Theory and Practice*. New York: Wiley, 1952.

Spartaco Caniggia (M'97) was born in Venice, Italy, in 1948. He received the Laurea degree in electronic engineering from the University of Padua, Padua, Italy, in 1972.

In 1975, after military service, he joined Siemens/Italtel, Milan, Italy, where he retired as a Physical Design and Electromagnetic Interference/Electromagnetic Compatibility (EMI/EMC) Manager for the Business Unit Products in 2005. He was a part-time Lecturer with the University of Rome "La Sapienza," L'Aquila, Milan, and Turin for signal integrity and EMC activities. From 2002 to 2004, he was with the EMC consortium of the University of Missouri-Rolla, Rolla. He is currently an EMC consultant. His research interests included the development of computer-aided design tools for SI and EMC; mathematical models for electrostatic discharge, shielding, grounding and wiring; methods for designing and testing information technology equipment to comply with EMC standards. He is the author of about 50 technical papers published in several journals and conference proceedings.

Dr. Caniggia received the Oral Presentation First Best Paper Award at the National EMC Symposium in 1988 and the Oral Presentation Second Best Paper Award at the IEEE International Symposium on Electromagnetic Compatibility in 1996. He is a member of working group SC77B MT12 of the International Electrotechnical Commission for electrostatic discharge.

Francescaromana Maradei (M'96–SM'06) was born in 1969. She received the Laurea degree in electrical engineering (*cum laude*) from the University of Rome "La Sapienza," Rome, Italy, in 1992, the Diplome d'Etudes Approfondies (DEA) in electrical engineering from the Institut National Polytechnique de Grenoble, Laboratoire d'Electrotechnique de Grenoble, Grenoble, France, in 1993, and the Ph.D. degree in Electrical Engineering from the University of Rome "La Sapienza," in 1997.

She joined the Department of Electrical Engineering, University of Rome "La Sapienza" in 1996, where she is currently an Associate Professor. Her main research interests include numerical techniques and their application to EMC problems (shielding and transmission line analysis).

Prof. Maradei received the James Melcher Price Paper Award, the Oral Presentation Best Paper Award at the International Symposium on Electromagnetic Compatibility in 1994, and the Poster Presentation Best Paper Award at the International Symposium on Electromagnetic Compatibility in 2000. She is a member of the Board of Directors of the IEEE Electromagnetic Compatibility Society, where she is also serving as Chapter Coordinator. From 1999 to 2000, she was an Associate Editor of the IEEE TRANSACTIONS ON ELECTROMAGNETIC COMPATIBILITY. Since 1998, she has been a member of the Editorial Board of the IEEE Conference on Electromagnetic Field Computation and the IEEE COMPUMAG Conference.